Wave Motion 97 (2020) 102581

Contents lists available at ScienceDirect

Wave Motion

journal homepage: www.elsevier.com/locate/wamot

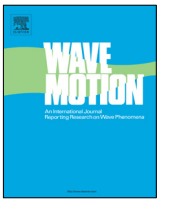

New solutions of the C.S.Y. equation reveal increases in freak wave occurrence

David Andrade *, Michael Stiassnie

Department of Civil and Environmental Engineering, Technion, Haifa, Israel

ARTICLE INFO

Article history:
Received 31 December 2019
Received in revised form 19 March 2020
Accepted 2 May 2020
Available online 15 May 2020

Keywords:
Water waves
JONSWAP spectrum
Freak waves

ABSTRACT

In this article we study the time evolution of broad banded, random inhomogeneous fields of deep water waves. Our study is based on solutions of the equation derived by **C**rawford, **S**affman and **Y**uen in 1980, (Crawford et al., 1980). Our main result is that there is a significant increase in the probability of freak wave occurrence than that predicted from the Rayleigh distribution. This result follows from the investigation of three related aspects. First, we study the instability of JONSWAP spectra to inhomogeneous disturbances whereby establishing a wider instability region than that predicted by Alber's equation. Second, we study the long time evolution of such instabilities. We observe that, during the evolution, the variance of the free surface elevation and thus, the energy in the wave field, localizes in regions of space and time. Last, we compute the probabilities of encountering freak waves and compare it with predictions obtained from Alber's equation and the Rayleigh distribution.

1. Introduction

This article deals with inhomogeneous fields of random deep water waves, as they are considered to be the breeding ground for extreme events, such as freak waves.

The study of inhomogeneous fields of random deep water waves begins in the late 70's with the work of Alber [1]. There, starting from the non linear Schrödinger equation for water waves, Alber derives an equation that governs the time evolution of two point correlations of the free surface elevation. This equation now bears his name, the Alber equation.

Upon linearizing his equation, around an initial Gaussian spectrum, Alber finds that the spectrum is unstable to inhomogeneous disturbances provided that it is narrow. Moreover, he shows that, as the spectrum broadens it inevitably stabilizes. No long time evolution of the correlation was performed at that time.

The first long time dependent solutions of Alber's equation were given by Stiassnie, Regev and Agnon in [2]. They considered three different types of spectra, a square, a Lorentz and a Gaussian spectrum and found that, in any case, the spectrum stabilizes when it broadens. Then, by computing the time evolution of the initial spectra, subjected to a small initial inhomogeneous disturbance, it was found that the variance of the free surface elevation appears periodic in time. This periodicity is regarded as the stochastic counterpart of the Fermi–Ulam–Pasta recurrence.

The determination of the evolution of the variance of the free surface enables the computation of the probability of encountering freak waves in the wave field. Indeed it was found by Regev, Agnon, Stiassnie and Gramstad in [3] that the probability of finding freak waves higher than twice the significant wave height is increased by a factor of 20 with respect

* Corresponding author.
E-mail addresses: deandradep@gmail.com (D. Andrade), miky@technion.ac.il (M. Stiassnie).

https://doi.org/10.1016/j.wavemoti.2020.102581
0165-2125/

to predictions based on the Rayleigh distribution. For extreme events of waves higher than three times the significant wave height the probability is increased by a factor of 30 000 which renders their encounter feasible.

With the aim of making realistic predictions Ribal, Babanin, Young, Toffoli and Stiassnie in [4] investigated the stability of the JONSWAP spectrum. Then, akin to [2], they found that, in case of instability, the subsequent time evolution is recurrent. The time evolutions enabled them to establish the probabilities of encountering freak waves and again it was many times higher than predictions by the Rayleigh distribution. Their main result is that the stability of the spectrum and the time–space periodicity of the solutions depend solely on a dimensionless width parameter Π_1. Recent improvements of these results, in particular regarding the stability region, were obtained by Gramstad in [5].

Recently Athanassoulis, Athanassoulis, Ptashnyk and Sapsis in [6] established a Landau damping mechanism for Alber's equation, analogous to that of plasma physics. This means that in case the spectrum is stable any inhomogeneous disturbance vanishes over time. Their methods allowed them to compute the instability boundary, for JONSWAP spectra, accurately. Their result is in good agreement with those previously mentioned.

There are two main results that summarize our current understanding of inhomogeneous deep water waves. The first one is that narrow spectra are unstable and they stabilize as their width broadens. The second one is that the probability of extreme waves is significantly increased in this case.

So far the first result has the caveat that it has been established by means of a narrow banded model, the Alber equation, which formally is not valid for broad spectrum. This leads to the main objective of this article, to free ourselves from the narrow band constraint and study the instability of the spectra, its time evolution and its impact on the probability of the freak waves, using a broad band model for inhomogeneous wave fields.

The model that we are going to use was derived by Crawford, Saffman and Yuen [7] in 1980. Here on referred to as the C.S.Y. equation. Their model follows directly from the Zakharov equation for the deterministic, non-linear, evolution of gravity waves, see Mei et al. [8]:

$$\frac{\partial B}{\partial t}(\mathbf{k}_0, t) = -i \iiint T_{0,m,n,p}\ \delta^{n,p}_{0,m}\ e^{i\Delta^{n,p}_{0,m} t}\ B^*_m B_n B_p\ d\mathbf{k}_m \mathbf{k}_n \mathbf{k}_p, \tag{1}$$

where subscripts denote a wave vector, so $B_j = B(\mathbf{k}_j, t)$, $*$ denotes the complex conjugate, and unless explicitly stated, the limits of integration are from $-\infty$ to ∞.

Then, the two wave number one-time spectral correlation function is introduced

$$R_{ij} = \langle B_i B^*_j \rangle, \tag{2}$$

where $\langle\cdot\rangle$ denotes an ensemble average. We further mention a fourth order average that is used in [7] throughout the derivation of the model

$$\langle B^*_j B^*_m B_n B_p \rangle = R_{nj} R_{pm} + R_{pj} R_{nm}. \tag{3}$$

The C.S.Y. equation is more general than Alber's. Indeed in [7] the authors showed that one can recover the latter from their model by means of a standard asymptotic approximation. Such approximation happens to be similar to the one used to derive the N.L.S. from Zakharov's equation. The main hypothesis behind the approximation is that the wave field is concentrated around a specific wave vector. This enables a simplification of the kernel and, upon a Taylor expansion, the integro-differential equation reduces to a differential equation.

This paper has three goals. First, through a linear stability analysis we investigate the instabilities of JONSWAP spectra to small inhomogeneous disturbances. This is in the same spirit as the early investigation using Alber's equation. The linearized form of equations already appears in [9] by Stuhlmeier, Vrecica and Toledo. Its earliest use was in determining the instabilities of degenerated quartets of waves by Stuhlmeier and Stiassnie in [10]. Here we take a slightly different form of the linear equations and use them to establish a correspondence between the wave number and growth rate of the inhomogeneous disturbance.

Once the instabilities of the spectra are established, we turn to their long time evolution, using numerical solutions of the C.S.Y. equation, and the JONSWAP spectra as initial data. To the best of our knowledge, this is the first time that many-mode solutions of the C.S.Y. equation are computed (as opposed to the three mode solutions of Stuhlmeier and Stiassnie in [10]).

Finally we look at the probability of encountering freaks waves. Our results predict an increase in the probabilities when compared to those of a homogeneous sea state, and are somewhat larger than those established by means of Alber's equation in [4] by Ribal et al.

2. On some properties of the C.S.Y. equation

Our starting point is the following equation derived by Crawford, Saffman and Yuen [7] for the time evolution of random, inhomogeneous, non-linear, gravity waves in deep water:

$$\begin{aligned}\frac{d}{dt}R_{ij} = &-2i \iiint T_{i,m,n,p}\ \delta^{n,p}_{i,m}\ e^{i\Delta^{n,p}_{i,m} t}\ R_{nj} R_{pm}\ d\mathbf{k}_m \mathbf{k}_n \mathbf{k}_p \\ &+\ 2i \iiint T_{j,m,n,p}\ \delta^{n,p}_{j,m}\ e^{-i\Delta^{n,p}_{j,m} t}\ R_{in} R_{mp}\ d\mathbf{k}_m \mathbf{k}_n \mathbf{k}_p.\end{aligned} \tag{4}$$

Akin to the Zakharov equation the evolution of the stochastic system is driven by four wave near resonant interactions. The wavenumber resonance condition is evident from the argument of the Dirac delta function $\delta^{n,p}_{i,m} = \delta(\mathbf{k}_i + \mathbf{k}_m - \mathbf{k}_n - \mathbf{k}_p)$, while the frequency detuning $\Delta^{n,p}_{i,m} = \omega(\mathbf{k}_i) + \omega(\mathbf{k}_m) - \omega(\mathbf{k}_n) - \omega(\mathbf{k}_p)$ marks the departure from exact resonance. Throughout this article the linear dispersion relation for deep water waves, $\omega(\mathbf{k}) = \sqrt{g|\mathbf{k}|}$, is used together with the kernel $T_{i,m,n,p} = T(\mathbf{k}_i, \mathbf{k}_m, \mathbf{k}_n, \mathbf{k}_p)$ given by Mei et al. [8] and Krasitskii [11].

Throughout this article we use the discretized version of (4) which can be obtained by assuming that the wave field has N different wave vectors $\mathbf{k}_1, \ldots, \mathbf{k}_N$ and that the correlation function has the form

$$R_{ij}(t) = \sum_{m,n=1}^{N} R_{mn}(t)\delta(\mathbf{k}_m - \mathbf{k}_i)\delta(\mathbf{k}_n - \mathbf{k}_j), \tag{5}$$

where R_{mn} is a complex variables and δ is the Dirac's delta function.

The Hermitian symmetry of the correlation function $R_{ij}(t)$transfers to the discrete correlations through the relation

$$R_{mn}(t) = R^*_{nm}(t). \tag{6}$$

Substituting (5) into (4) reduces the integro-differential equation into the following non-linear system of O.D.Es:

$$\begin{aligned}\frac{d}{dt}R_{ij} = -2i \sum_{m,n,p=1}^{N} T_{i,m,n,p}\, \delta^{n,p}_{i,m}\, e^{i\Delta^{n,p}_{i,m}t}\, R_{nj}R_{pm} \\ + 2i \sum_{m,n,p=1}^{N} T_{j,m,n,p}\, \delta^{n,p}_{j,m}\, e^{-i\Delta^{n,p}_{j,m}t}\, R_{in}R_{mp}, \quad \text{for } i,j = 1,2,\ldots,N.\end{aligned} \tag{7}$$

In (7) each of the summation variables m, n and p range from 1 to N and $\delta^{n,p}_{j,m}$ stands now for the Kronecker delta,

$$\delta^{n,p}_{j,m} = \begin{cases} 1 & \text{if } \mathbf{k}_j + \mathbf{k}_m = \mathbf{k}_n + \mathbf{k}_p. \\ 0 & \text{otherwise.} \end{cases} \tag{8}$$

The objective of this article is to study equation (7) and its solutions.

2.1. Invariants of the C.S.Y. equation

The original Zakharov (1) equation has three invariants of motion; wave action, momentum and Hamiltonian, see [8, equation 14.3.14]. Upon ensemble averaging we find that wave action and momentum, A and $\mathbf{M}$ respectively, are conserved. The derivation of the third invariant $\tilde{H}$ is more elaborate but it includes the ensemble average of the original Hamiltonian. The conserved quantities are:

$$A = \sum_{j=1}^{N} R_{jj}. \tag{9}$$

$$\mathbf{M} = \sum_{j=1}^{N} \mathbf{k}_j R_{jj}. \tag{10}$$

$$\tilde{H} = \sum_{j=1}^{N} \omega_j R_{jj} - \mathrm{Im}\left[\sum_{j,m,n,p=1}^{N} T_{j,m,n,p}\delta^{n,p}_{j,m}\Delta^{n,p}_{j,m} \int_0^t e^{i\Delta^{n,p}_{j,m}s} R_{nj}R_{pm}\, ds \right]. \tag{11}$$

The proof that these quantities are conserved can be obtained from the author.

These invariants are general as they do not depend on the configuration of the waves $\mathbf{k}_1, \ldots, \mathbf{k}_N$ within the wave field. Moreover by replacing the sums by integrals over the whole $\mathbf{k}$-space, we obtain their counterparts for the continuous C.S.Y. Eq. (4). Here we use them to monitor our numerical solutions.

2.2. Homogeneous solutions of the C.S.Y. equation

We say that the wave field is homogeneous if

$$R_{ij} = C_j\delta^j_i = \begin{cases} C_j & \text{if } \mathbf{k}_j = \mathbf{k}_j. \\ 0 & \text{otherwise.} \end{cases} \tag{12}$$

By a homogeneous solution of the system (7) we mean a solution that satisfies (12) for all time.

As we show next, any homogeneous solution is stationary. Indeed, let R be a homogeneous solution of (7). Then substituting (12) into any of the sums in the right hand side of (7) yields that

$$\sum_{m,n,p} T_{i,m,n,p}\,\delta^{n,p}_{i,m}\,e^{i\Delta^{n,p}_{i,m}t}\,R_{nj}R_{pm} = \begin{cases} -2iC_i\sum_m T_{i,m,i,m}\,C_m & \text{if } i=j,\\ 0 & \text{if } i\neq j.\end{cases}$$

And therefore, the right hand side of (7) vanishes. This implies that for any homogeneous solution $dR_{ij}/dt = 0$, as claimed.

There are two consequences of this fact. The first one is that the C.S.Y. does not create inhomogeneities. If at some instant t_0 $R(t_0)$ is homogeneous then, by the theorem of uniqueness of solutions of ordinary differential equations, it follows that $R(t) = R(t_0)$ for all t. In particular

$$R_{ij} = \begin{cases} C_j & \text{a non negative real constant for } i=j.\\ 0 & \text{for } i\neq j.\end{cases} \tag{13}$$

The second consequence is that nontrivial evolution is only possible when there are inhomogeneous terms in the initial conditions. Hence, the natural question that arises is how stable are homogeneous solutions to small initial inhomogeneous disturbances?

We turn to this question in the next subsection.

2.3. Linear stability analysis of the C.S.Y. equation

We begin by introducing the following change of variables

$$r_{ij} = R_{ij}e^{-i(\omega_i-\omega_j)t}, \tag{14}$$

and, after substituting into (7), we obtain

$$\begin{aligned}\frac{d}{dt}r_{ij} = &-i\left(\omega_i-\omega_j\right)r_{ij} - 2i\sum_{m,n,p} T_{i,m,n,p}\,\delta^{n,p}_{i,m}\,r_{nj}r_{pm}\\ &+ 2i\sum_{m,n,p} T_{j,m,n,p}\,\delta^{n,p}_{j,m}\,r_{in}r_{mp}.\end{aligned} \tag{15}$$

The linear stability analysis begins by looking for asymptotic solutions of the form

$$r_{ij}(t) = C_j(t)\delta^j_i + \mu r^1_{ij}(t) + \mathcal{O}(\mu^2), \tag{16}$$

where μ is a small parameter controlling the inhomogeneous disturbance r^1_{ij}. Next we substitute (16) into (15) and collect the terms in powers of μ. At leading order ($\mu = 0$) we find that the right hand side of (15) vanishes leaving that

$$\frac{d}{dt}C_j = 0, \tag{17}$$

and thus, it is constant. This set of values are called the initial homogeneous wave action spectrum.

At next order $\mathcal{O}(\mu)$ we obtain that, for $i = j$,

$$\frac{d}{dt}r^1_{ij} = 0. \tag{18}$$

Without loss of generality we set r^1_{jj} to be zero.

However when $i \neq j$ we get the following linear system of equations which can be compactly written as

$$\frac{d}{dt}r^1_{ij} = -i\left(\Omega_i-\Omega_j\right)r^1_{ij} + 2i(C_i-C_j)\sum_{m,n=1}^{N} T_{i,m,j,n}\,\delta^{j,n}_{i,m}r^1_{nm}, \tag{19}$$

for $i, j = 1, 2, \ldots, N$ and where Ω is

$$\Omega_j = \omega_j + 2\sum_{m=1}^{N} T_{j,m,j,m}\,C_m. \tag{20}$$

We call equation (19) the linearized CSY equation. It governs the short time evolution of initial inhomogeneous disturbances of a given homogeneous spectra C_j. An equivalent form of this equation was derived by Stuhlmeier, Vrecica and Toledo in [9].

With this equation at hand, we study the instability of a homogeneous spectra C_j. To this end we look for solutions of (19) of the form

$$r^1_{ij}(t) = e^{\lambda t}r^1_{ij}(0), \tag{21}$$

where λ is a complex number and $r^1_{ij}(0)$ is an initial inhomogeneous disturbance. Substituting (21) into (19) yields

$$\begin{aligned}\frac{d}{dt}r^1_{ij}(t) =&\lambda r^1_{ij}(t) = \lambda e^{\lambda t} r^1_{ij}(0) = \\ &- i(\Omega_i - \Omega_j)e^{\lambda t} r^1_{ij}(0) + 2i(C_i - C_j)\sum_{m,n=1}^{N} T_{i,m,j,n}\,\delta^{j,n}_{i,m} e^{\lambda t}\, r^1_{nm}(0),\end{aligned} \tag{22}$$

that shows the fundamental relation between λ and $r^1_{ij}(0)$:

$$\left(\lambda + i(\Omega_i - \Omega_j)\right) r^1_{ij}(0) - 2i(C_i - C_j)\sum_{m,n=1}^{N} T_{i,m,j,n}\,\delta^{j,n}_{i,m}\, r^1_{nm}(0) = 0, \tag{23}$$

for all $i, j = 1, 2, \ldots, N$.

Eq. (23) is a homogeneous system of N^2 linear equations for $r^1_{ij}(0)$. Such systems only have nontrivial solutions when their determinant is zero. Such determinant turns into an N^2 algebraic equation for λ. Moreover one can see that a necessary and sufficient condition for (21) to be a solution of (19) is that λ and $r^1_{ij}(0)$ satisfy (23). Note that in this way we reduced the problem of finding solutions of systems of differential equations to finding eigenvalues and eigenvectors of systems of linear equations.

Once we have determined λ and $r^1_{ij}(0)$ (21) gives a solution of (19). Its qualitative behavior is controlled by the real part of λ. When it is positive, the solution grows exponentially and when it is negative, the solution decays exponentially to zero. Hence we define the growth rate to be:

$$\Omega = \mathrm{Re}[\lambda]. \tag{24}$$

We say that the original spectrum C_j is unstable if it has at least one non-zero growth rate. Otherwise we say that it is stable.

3. Relation between wave numbers and growth rates

One of the attractive features of the C.S.Y. equation is that Alber's equation can be derived from it in the narrow band limit. For Alber's equation, it turns out that the growth rates are determined as solutions of a single equation, see equation (4.16) in [1] or equation (2.17) in [2]. Such an equation defines a correspondence between wave vectors and growth rates $\Omega(K)$ which is a kind of "dispersion relation".

In the C.S.Y. equation we have not found any generalization of such equation. However it is possible to establish a correspondence between wave numbers and growth rates. This is the main content of this section.

From here and to the end of this article, we restrict ourselves to unidirectional waves. The wave numbers of the spectra are evenly spaced:

$$0 \le k_1 < \cdots < k_N, \tag{25}$$

with $k_{j+1} - k_j = dk$, for all $j = 1, \ldots, N-1$.

The key observation that will allow us to set up the correspondence between K and Ω is that the linear C.S.Y. equation (19) decouples into several smaller systems of linear equations. To show this, fix a wave vector K and rewrite the Kronecker delta as

$$\delta^{j,n}_{i,m} = \sum_u \delta^u_{i-j}\delta^{n-m}_u. \tag{26}$$

Then substituting this form of the delta in (19) yields

$$\frac{d}{dt}r_{ij} = -i\left(\Omega_i - \Omega_j\right) r_{ij} + 2i\sum_u \delta^u_{i-j}(C_i - C_j)\sum_{m,n=1}^{N} T_{i,m,j,n}\,\delta^{n-m}_u r_{nm}, \tag{27}$$

for all $i, j = 1, 2, \ldots, N$.

Multiplying both sides of (27) by δ^K_{i-j} [1] one obtains the following equation where only the terms r_{nm} with $k_n - k_m = K$ are involved

$$\frac{d}{dt}\delta^K_{i-j}r_{ij} = -i\left(\Omega_i - \Omega_j\right)\delta^K_{i-j}r_{ij} + 2i\delta^K_{i-j}(C_i - C_j)\sum_{m,n=1}^{N} T_{i,m,j,n}\,\delta^{n-m}_K r_{nm}. \tag{28}$$

We point out that Eq. (28) does not represent a single system of equations; it represents a family of linear systems of differential equations parametrized by K.

[1] δ^K_{i-j} is the Kronecker delta that vanishes unless $k_i - k_j = K$.

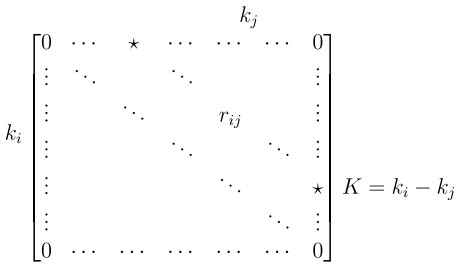

Fig. 1. Schematic representation of $\delta^K_{i-j} r_{ij}$. Only the terms along the diagonal $K = k_i - k_j$ are the ones that participate in the linear system of Eqs. (28) and (29). Each diagonal defines an independent system of equations and so, a unique positive growth rate $\Omega(K)$.

In Fig. 1 we give a schematic representation of the situation; all the terms r_{ij} along the diagonal $K = k_i - k_j$ interact only with themselves through equation (28). Therefore, instead of solving (19) for all r_{ij}, we need only solve (28) for each K separately.

Respectively, the eigenvalues of the system (23) also split into the following family of independent linear equations:

$$\lambda \delta^K_{i-j} r^1_{ij}(0) = -i(\Omega_i - \Omega_j)\delta^K_{i-j} r^1_{ij}(0) + 2i\delta^K_{i-j}(C_i - C_j) \sum_{m,n=1}^{N} T_{i,m,j,n}\, \delta^{j,n}_{i,m}\, r^1_{nm}(0). \tag{29}$$

Note that for any K the system (29) has a finite set of eigenvalues and the set of all the eigenvalues of (23) is the union of the sets of eigenvalues of each system.

In the investigations that we present in this article it was always the case that each system happens to have at most one positive growth rate. This defines a correspondence between K and Ω

$$K \longmapsto \Omega(K) = \text{unique positive growth rate of (29)}. \tag{30}$$

One of the main advantages of decoupling the C.S.Y. equation is that it allows for an efficient computation of the growth rates.

4. Stability analysis of JONSWAP spectra

From here on we consider the unidirectional JONSWAP spectrum presented as a function of the wave number. Its standard form is, see [4]:

$$S(k) = \frac{\alpha}{2k^3} \exp\left[-\frac{5}{4}\left(\frac{k}{k_p}\right)^{-2}\right] \gamma^{\exp\left[-\left(\sqrt{\frac{k}{k_p}}-1\right)^2/2\sigma^2\right]}. \tag{31}$$

In this formula k_p denotes the peak wave in the spectrum. The parameter σ is the peak width and the parameters γ and α are the peak enhancement factor and the energy scale of the spectrum, respectively. We set $\sigma = 0.08$, $k_p = 1\ \mathrm{m}^{-1}$ and $g = 9.81\ \mathrm{m\ s}^{-2}$.

Following Ribal et al. [4] we consider the dimensionless width parameter

$$\Pi_1 = \frac{\varepsilon}{\alpha\gamma}, \tag{32}$$

where the steepness parameter is

$$\varepsilon = k_p \sqrt{2 \int_0^\infty S(k)\, dk}, \tag{33}$$

in accordance with Ribal et al. and Stiassnie et al. [2,4].

4.1. Homogeneous wave action spectra

In order to initialize the computations we need the initial wave action homogeneous spectrum $R_{ij} = C_j \delta^j_i$. This is obtained from the JONSWAP spectra as follows. Starting from a JONSWAP spectra, the variance of the amplitude a_j, of the wave k_j, is computed from the following formula, see Holthuijsen [12]:

$$\frac{\langle a_j^2 \rangle}{2} = \int_{k_j}^{k_j + dk} S(k)\, dk \approx dk S(k_j). \tag{34}$$

On the other hand, in the Zakharov equation, the amplitude a_j of the wave k_j is

$$a_j^2 = \frac{\omega_j}{2g\pi^2}|B_j|^2, \tag{35}$$

where upon averaging yields

$$\langle a_j^2 \rangle = \frac{\omega_j}{2g\pi^2}C_j. \tag{36}$$

From these formulas we obtain the desired relation between the energy spectrum S and the wave action spectrum C

$$C_j = \frac{4g\pi^2 dk}{\omega_j}S(k_j). \tag{37}$$

4.2. Instability of the JONSWAP spectra

We study the instability of the JONSWAP spectra to small inhomogeneous disturbances. Since the values of σ and k_p are fixed, we are left with two free parameters γ and α to determine the spectral shape. We aim to find the instability region in the (γ, α) plane.

As we have already shown, each spectra has its own dispersion relation $\Omega(K)$ which determines its instability. Indeed a spectra is stable whenever $\Omega(K)$ vanishes identically and unstable if for some K, $\Omega(K) > 0$. Let:

$$\Omega^{(max)} = \max_k \Omega(k). \tag{38}$$

Then the spectrum is unstable if and only if $\Omega^{(max)} > 0$ and stable otherwise.

In case of instability one computes the growth rates $\Omega(K)$, then one finds their corresponding $\Omega^{(max)}$ and $K^{(max)}$, the wave number of the inhomogeneous disturbance, where the maximum is attained; it is the most unstable wave number.

As in [2,4], we render all the growth rates and wave numbers dimensionless by means of

$$\tilde{\Omega} = \Omega/\varepsilon^2\omega_p, \tag{39}$$

$$\tilde{K} = K/\varepsilon k_p. \tag{40}$$

In Fig. 2a we plot the instability region of the JONSWAP spectra in the (γ, α) plane.

On the left panel of Fig. 2a the red solid lines are the level lines of $\tilde{\Omega}^{(max)}$. On the right panel we have their corresponding most unstable wave number $\tilde{K}^{(max)}$. The level lines on the right panel (for the wave numbers) were slightly smoothed in order to get a clearer picture.

By looking at the growth rates, we see that larger values of $\tilde{\Omega}^{(max)}$ happen for larger values of γ which corresponds to narrow spectra. On the other hand, when γ tends to 1, $\tilde{\Omega}^{(max)}$ tends to 0 (stability). This values correspond to broad spectra. Thus, our computations confirm that narrow spectra is prone to instability whereas broad spectra is stable.

We compare our results with those obtained by Ribal et al. in [4]. Their criteria for instability, their growth rates and their corresponding most unstable wave numbers, are all given in terms of the dimensionless width parameter Π_1. The largest growth rate $\tilde{\Omega}_1^{(max)}$ and most unstable wave number, denoted by them as $\tilde{P}_1^{(max)}$, satisfy the equations

$$\tilde{P}_1^{(max)} = 2.313 - 0.976\Pi_1, \tag{41}$$

$$\tilde{\Omega}_1^{(max)} = 0.572 - 0.557\Pi_1. \tag{42}$$

There is instability when $\tilde{\Omega}_1^{(max)} > 0$. Thus the instability boundary is determined by $\tilde{\Omega}_1^{(max)} = 0$, that leads to $\Pi_1 = 1.0269$. On the other hand Gramstad's proposed instability boundary is obtained by setting $\Pi_1 = 1.2987$ [5]. In both panels of Fig. 2a the instability boundary of Ribal et al. is plotted in the thick blue dashed line, whereas Gramstad's instability boundary is plotted in the red dotted line.

In Fig. 2a the thin blue dashed lines show the results of Ribal et al. On the left panel we plot the level lines of $\tilde{\Omega}_1^{(max)}$ and on the right panel we plot the level lines of $\tilde{P}_1^{(max)}$. Note that the stability region obtained with Alber's equation is smaller than the one predicted by the C.S.Y. equation.

Now we focus on four cases which are summarized in Table 1. Case a, which is identical to case B_4, studied by Ribal et al. in [4] and serves to compare both models. Case b which corresponds to our new fastest growth rate. Cases c and d are unstable for the C.S.Y. equation however case c is between the instability boundaries for Alber's equation and case d is stable according to both predictions.

On the left panel of Fig. 2b we plot the different JONSWAP spectra. On the right one, we plot their respective growth rates $\tilde{\Omega}$ as a function of $\tilde{K}$. The blue solid lines correspond to case a, the yellow dotted line to case b, the red broken line to case c and the purple broken line with circles to case d.

5. Long time evolution

In this section we study the evolution of cases a, b, c, and d triggered by a small inhomogeneous disturbance.

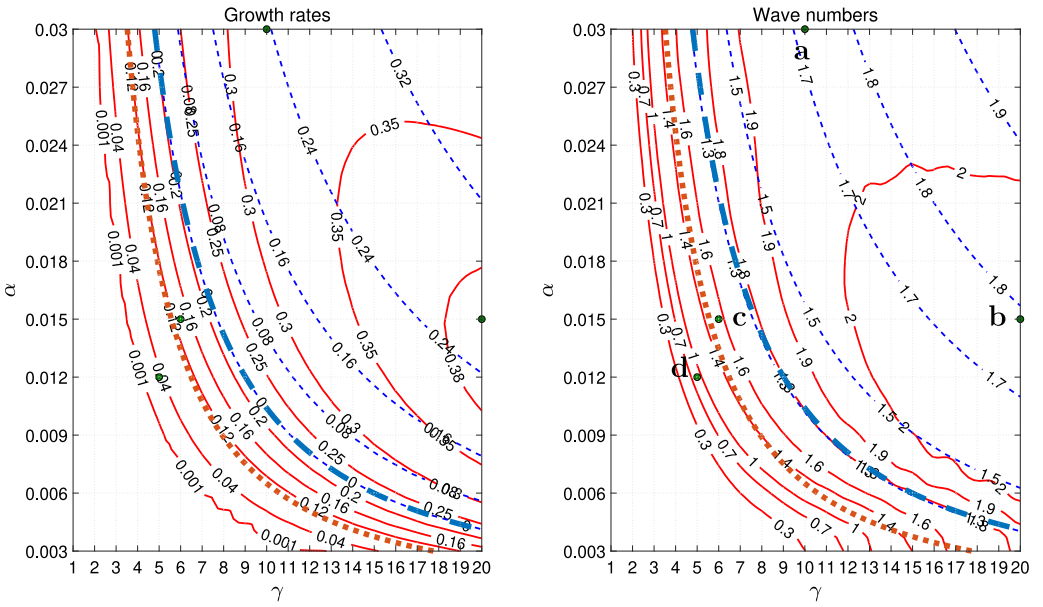

(a) Left panel: The rel solid lines are a contour plot of the maximum growth rate $\tilde{\Omega}^{(max)}$ predicted by the C.S.Y. equation. The blue dashed lines are the contours of $\tilde{\Omega}_1^{(max)}$ computed from (42). Right panel: The red solid lines are the level lines of the most unstable wave number $\tilde{K}^{(max)}$, according to the C.S.Y. equation. The blue dashed lines are the contours of the most unstable wave number $\tilde{P_1}^{(max)}$, according to (41). The red lines in the right panel were smoothed out. In both figures the blue dashed line corresponds to the stability boundary $\Pi_1 = 1.0269$ of Ribal et al., and the red dotted line is the stability boundary $\Pi_1 = 1.29872$ of Gramstad.

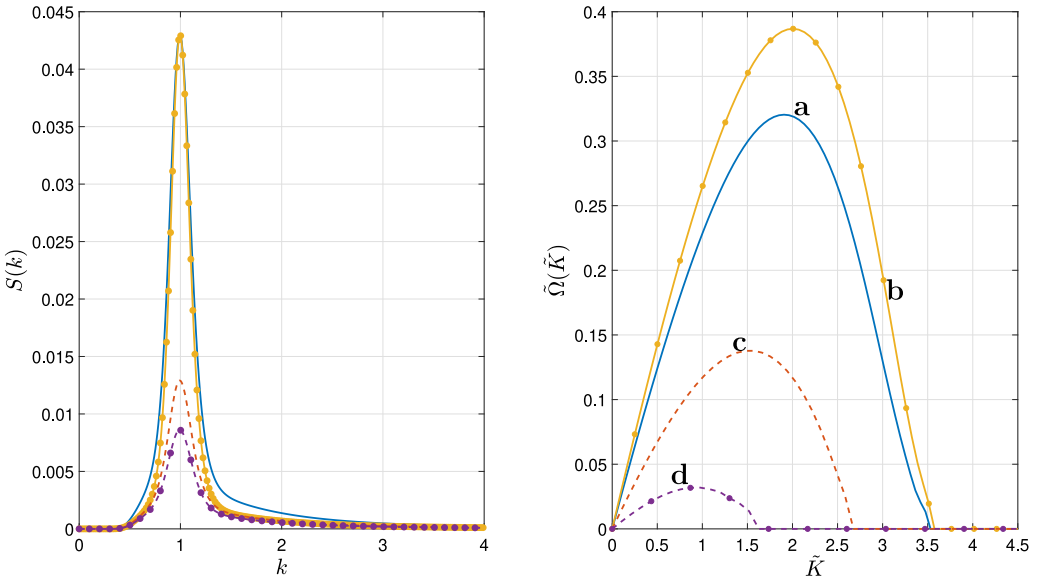

(b) Left panel: Shapes of the JONSWAP spectra for each case. Right panel: Plot of the growth rates $\tilde{\Omega}$ as a function of wave number $\tilde{K}$. The blue solid lines correspond to case a. The yellow dotted line corresponds to case b. The red broken line is case c and the purple broken line with dots corresponds to case d.

Fig. 2. Linear stability analysis of JONSWAP spectra.

Table 1
Parameters of the JONSWAP spectra studied.

Cases	γ	α	ε	$\tilde{\Omega}^{(max)}$	$\tilde{K}^{(max)}$	Π_1
Case a	10	0.03	0.1789	0.3204	1.9061	0.5962
Case b	20	0.015	0.1598	0.3868	2.0070	0.5328
Case c	6	0.015	0.1086	0.1377	1.5690	1.2072
Case d	5	0.012	0.0925	0.0317	0.8674	1.5413

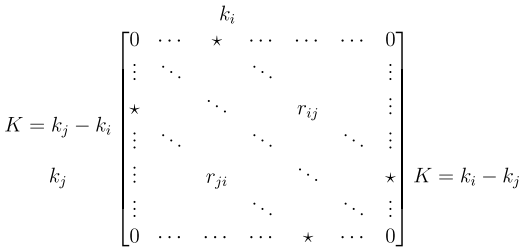

Fig. 3. Schematic representation of the eigenvector of the linearized C.S.Y. equation. Recall that $r_{ji} = r_{ij}^*$ and all the entries outside the diagonals $k_i - k_j = \pm K$ are zero.

5.1. Initial conditions

Let $R_{ij} = C_j\delta_i^j$ be the initial wave action spectra, given by formula (37), let $\Omega^{(max)}$ be its largest growth rate and $K^{(max)}$ be its most unstable wave number.

For the initial disturbance we start with $r_{ij}^1(0)$ a nonzero eigenvector for the eigenvalue λ, whose real part is the growth rate $\Omega^{(max)}$. Note that the structure of the linearized C.S.Y. equation imposes a structure on $r_{ij}^1(0)$. All its non-zero entries lie along the diagonal line $k_j - k_i = K^{(max)}$, see Fig. 3. Therefore one can write

$$r_{ij}^1(0) = f_i\delta_{j-i}^{K^{(max)}}, \quad \text{for } k_i = k_1, k_2, \ldots, k_N - K^{(max)}. \tag{43}$$

The eigenvector is computed using MATLAB's eig routine. Typically, it gives a unit vector ($\|f_i\|_2 = 1$), which has to be scaled before using it as an initial condition for the non linear solver.

In order to normalize f_i, first we make it comparable with the homogeneous spectra. Let

$$\|C_j\|_1 = \sum_j C_j, \tag{44}$$

$$\|f_i\|_1 = \sum_m |f_i|, \tag{45}$$

$$Q = \frac{\|C_j\|_1}{\|f_i\|_1}. \tag{46}$$

The scaling of f_i is achieved by setting

$$F_i = Qf_i. \tag{47}$$

Then, we introduce a small parameter μ, which controls the magnitude of the inhomogeneous disturbance. Finally the initial value for the non-linear evolution of the system is

$$R_{ij}(0) = C_j\delta_i^j + \mu\left(F_i\delta_{j-i}^{K^{(max)}} + F_i^*\delta_{j-i}^{-K^{(max)}}\right), \tag{48}$$

where the complex conjugate terms, along $k_j - k_i = -K^{(max)}$, are necessary to ensure the Hermitian symmetry of the C.S.Y. equation.

5.2. Numerical simulations

Evaluating the right hand side of Eq. (7) means that we have N^2 equations to determine all possible dR_{ij}/dt. Of course upon invoking the Hermitian symmetry, the number of equations reduces to $N(N+1)/2$. However each equation is defined as the difference of two three-fold sums. Fortunately, the Kronecker deltas cancel most of the terms that would appear otherwise. Nevertheless, the computation turns out to be expensive and, due to memory limitations, a grid of $N = 80$ evenly distributed wave numbers was used along the interval $[0, 4k_p]$. The time interval is set to $[t_0 = 0, t_f = 3000\ \text{s}]$ in all cases. This time corresponds to approximately 1500 periods of the peak wave $k_p = 1\ \text{m}^{-1}$.

Table 2
Invariants and their conservation for each of the examples treated. eA, $e\mathbf{M}$ and $e\tilde{H}$ are the maximum relative errors in the invariants A, $\mathbf{M}$ and $\tilde{H}$, respectively.

	Case a	Case b	Case c	Case d
A	1.9084	1.5460	0.6944	0.5003
$\mathbf{M}$	2.1057	1.6439	0.7934	0.5796
$\tilde{H}$	6.1952	4.9479	2.2857	1.6560
eA	1.8464×10^{-11}	7.3181×10^{-12}	1.1393×10^{-12}	7.9732×10^{-13}
$e\mathbf{M}$	2.5435×10^{-11}	1.8870×10^{-11}	2.8695×10^{-12}	2.1306×10^{-12}
$e\tilde{H}$	3.5950×10^{-6}	2.2219×10^{-6}	1.2238×10^{-7}	2.5103×10^{-8}

The initial homogeneous spectra is computed by means of formula (37). Then, once we have the largest growth rate $\Omega^{(max)}$ and its wave number $K^{(max)}$, the initial data follows from formula (48). In all the simulations the magnitude of the inhomogeneous disturbance is controlled by setting $\mu = 0.1$.

With initial data at hand we use MATLAB's ode113 to integrate the equations in time, using relative and absolute tolerances of 10^{-10}.

Once the time evolution is computed we check the conservation of the invariants. For the third invariant the time integral in formula (11) is approximated using the trapezoidal rule with a fixed time step of $dt = 0.3$ s.

Before going to the specific features captured by our numerical solutions, we observed that the time dependent solution also has a particular structure, that resembles that of the initial data. In all four cases studied herein we found that the solution is supported along specific diagonals defined by

$$k_i - k_j = nK^{(max)}, \tag{49}$$

where n is an integer. In other words, the values of R_{ij} are always zero whenever $k_i - k_j$ is not an integer multiple of $K^{(max)}$.

Initially the homogeneous spectrum is located along the main diagonal ($n = 0$) and its disturbance lies along the diagonals corresponding to $n = \pm 1$, in accordance with Fig. 3. Then, as a result of the non linear interactions, the solution propagates to all the other diagonals in the correlation matrix.

In Figs. 4a, 4b, 5a and 5b we plot the time average of the solution

$$\tilde{R}_{ij} = \frac{1}{t_f - t_0} \int_{t_0}^{t_f} |R_{ij}(s)| \, ds. \tag{50}$$

Each individual panel shows the time averaged solution along the diagonal $k_i - k_j = nK^{(max)}$ for $n = 0, 1, 2, 3, 4$ and 5. We put all the diagonals on the same coordinate system defined by $k_m = (k_i + k_j)/2$. In all the figures the red dashed line indicates the initial condition. On the panel corresponding to $n = 0$ we have the initial spectra and on the panel for $n = 1$, we see the modulus of the initial disturbance, as given by formula (48). Note that in all the other figures the initial data is zero.

By looking at the evolution of the homogeneous terms, the upper left panel in Figs. 4a, 4b, 5a and 5b we can distinguish between two different kinds of behavior. The first one, shared by cases a and b, is characterized by a dramatic change in the spectrum. In both cases we see a clear broadening of the homogeneous part of the spectrum and the time average reveals the formation of peaks at lower wave numbers throughout the evolution. Also, in both cases, there is significant growth of the initial disturbance which reaches values comparable to those of the homogeneous terms.

The second behavior, common to cases c and d, is far less drastic. Indeed, there is little change in the homogeneous terms or in the initial disturbance, see the first two panels in figures Figs. 5a and 5b, respectively.

In all four cases R_{ij} decays as one moves away from the main diagonal $k_i = k_j$. Nevertheless such decay is slower in cases a and b than in cases c and d. We also point out that there seems to be some sort of self similarity in the solution, i.e. in all four cases, the time average on any diagonal seems to be a scaling of that of the previous one.

Finally, the values of the invariants and their maximum relative errors, throughout the evolution, are given in Table 2.

5.3. Evolution of the variance of the free surface

Our results are easier to grasp when relating them to the variance of the free surface elevation. To this end we recall that, in the deterministic scenario, the leading order approximation of the free surface elevation is given by, see [8]

$$\eta = \frac{1}{2\pi} \sum_{j=1}^{N} \sqrt{\frac{\omega_j}{2g}} \left[B_j \, e^{i(k_j x - \omega_j t)} + c.c. \right] \tag{51}$$

From this formula, the variance of the free surface is

$$\rho(x, t) = \langle \eta^2 \rangle = \frac{1}{8g\pi^2} \sum_{i,j=1}^{N} \sqrt{\omega_i \omega_j} \left[R_{ij} \, e^{i((k_i - k_j)x - (\omega_i - \omega_j)t)} + c.c. \right] \tag{52}$$

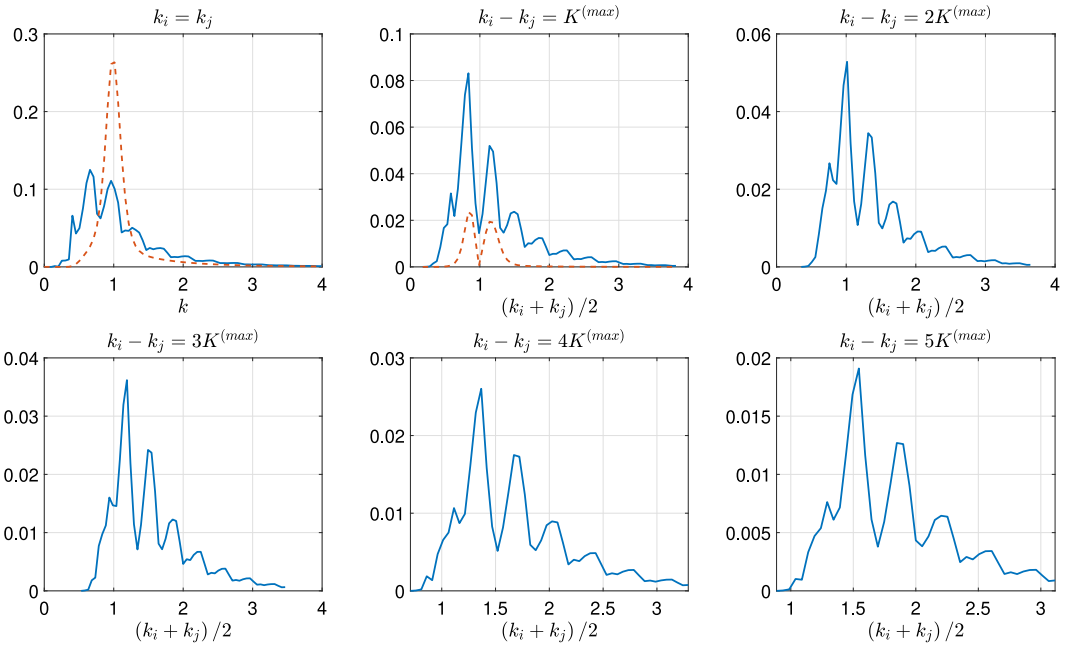

(a) Case a: Evolution of R_{ij} initialized by the JONSWAP spectrum with $\gamma = 10$ and $\alpha = 0.03$.

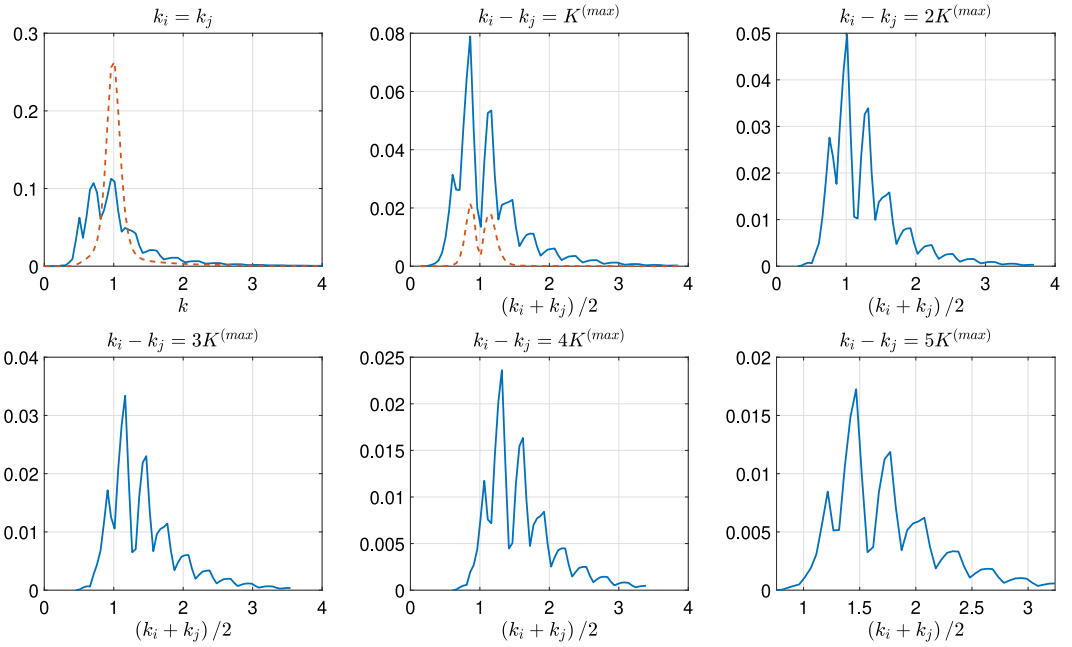

(b) Case b: Evolution of R_{ij} initialized by the JONSWAP spectrum with $\gamma = 20$ and $\alpha = 0.015$.

Fig. 4. Time averaged results of R_{ij}. Each panel displays the averaged spectral distribution for different values of $K = k_i - k_j$. The first one corresponds to $K = 0$, here we see the homogeneous spectra and the red line shows the shape of the initial JONSWAP spectrum. The second panel is for $K = K^{(max)}$. Here we see in red the initial disturbance. All the other panels correspond to integer multiples of $K^{(max)}$, specifically $K = nK^{(max)}$ for $n = 2, \ldots, 5$.

This variance is a periodic function of x. This is a consequence of the fact that, $R_{ij} = 0$ whenever $k_i - k_j$ is not an integer multiple of $K^{(max)}$. In case that $k_i - k_j = nK^{(max)}$ for some integer n, we can group the terms in (52) according to n. For

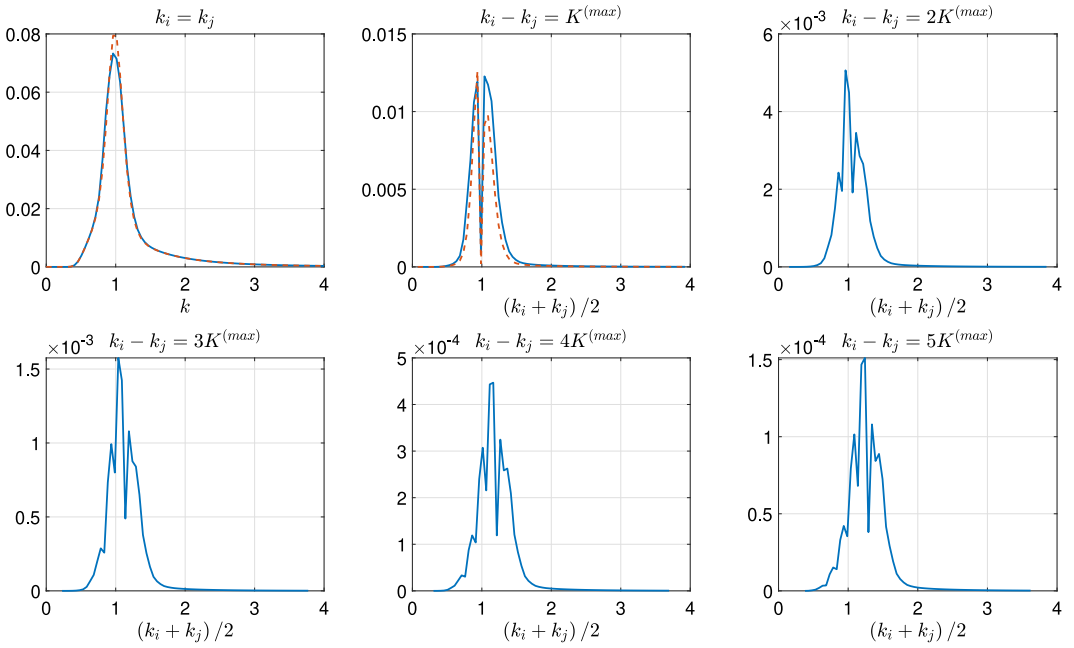

(a) Case c: Evolution of R_{ij} initialized by the JONSWAP spectrum with $\gamma = 6$ and $\alpha = 0.015$.

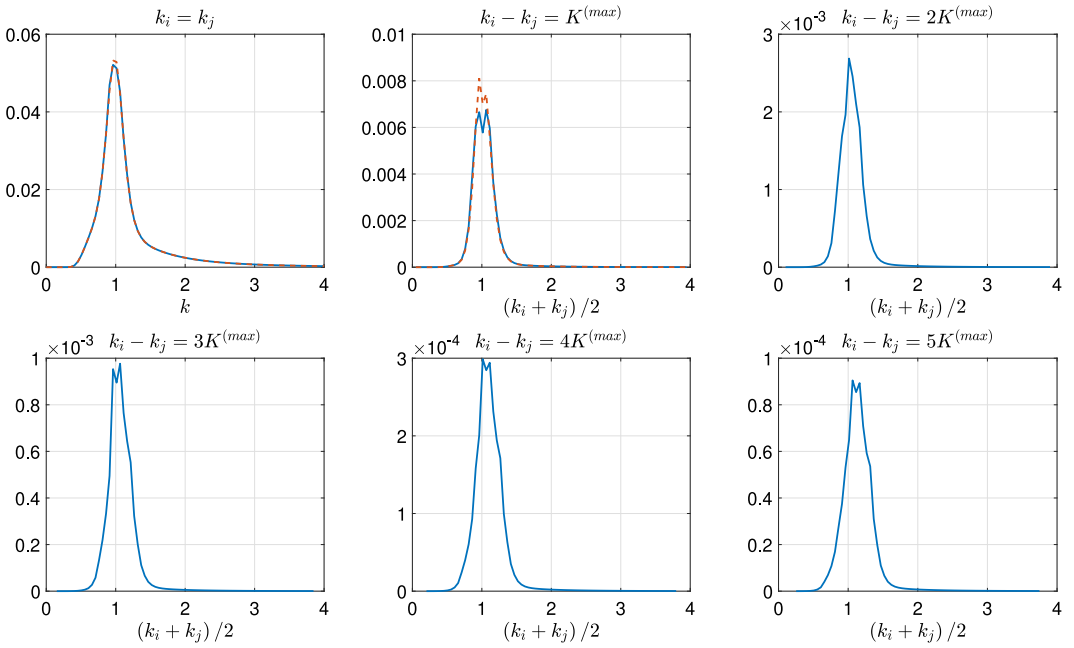

(b) Case d: Evolution of R_{ij} initialized by the JONSWAP spectrum with $\gamma = 5$ and $\alpha = 0.012$.

Fig. 5. Time averaged results of R_{ij}. Each panel displays the averaged spectral evolution for different values of $K = k_i - k_j$. The first one corresponds to $K = 0$, here we see the homogeneous spectra and the red line shows the shape of the initial JONSWAP spectrum. The second panel is for $K = K^{(max)}$. Here we see in red the initial disturbance. All the other panels correspond to integer multiples of $K^{(max)}$, specifically $K = nK^{(max)}$ for $n = 2, \ldots, 5$.

example when $n = 0$, the sum of all the terms such that $k_i = k_j$ is

$$F_0 = \frac{1}{4g\pi^2} \sum_j \omega_j R_{jj}(t). \tag{53}$$

In general, the sum of all the terms such that $k_i - k_j = nK^{(max)}$ is

$$F_n = \sum_{i=1}^{N-K} \sqrt{\omega_i \omega_{i+K}} R_{i,i+K}\, e^{-i(\omega_i - \omega_{i+K})t}, \tag{54}$$

which shows that ρ can be written as a superposition of harmonic waves

$$\rho = \frac{1}{8g\pi^2} \sum_{n=0}^{N-1} e^{ixnK^{(max)}} F_n + c.c, \tag{55}$$

and therefore it is a periodic function of x with period $2\pi/K^{(max)}$.

The fact that the variance is periodic in space is in agreement with a previous study of the C.S.Y. equation on degenerated quartets of waves made by Stuhlmeier and Stiassnie in [10]. Moreover it has also been observed in the solutions of the Alber equation, see [2–4].

For convenience we switch to dimensionless variables:

$$\tilde{x} = (\varepsilon k_p)x \tag{56}$$

$$\tilde{t} = (\varepsilon^2 \omega_p)t \tag{57}$$

$$\tilde{\rho} = \frac{k_p^2}{\varepsilon^2}\rho. \tag{58}$$

Note that ε is different for each spectra and its values are given in Table 1.

A snapshot of $\tilde{\rho}$ is given in Figs. 6a, 6b, 7a and 7b. In all cases the initial variance, plotted in the red broken line on the lower right panel, has a sinusoidal form, with mean value 0.5.

In Figs. 6a, 6b, 7a and 7b the leftmost panel is a surface plot of the variance $\tilde{\rho}$. The time window chosen was from $t = 1000$ s to $t = 1060$ s, however due to the fact that ε is different in all cases, the values of the dimensionless time variable $\tilde{t}$ are different as well. The spatial window is one period. On the right panels we have cross sections of it.

The two distinctive behaviors, already encountered in the time average of R_{ij}, can also be seen in the evolution $\tilde{\rho}$. This time cases a and b, which had a dramatic change in their spectra, reveal a localized form in their corresponding variances $\tilde{\rho}$. The values in the crests are about four times larger than the initial ones and the values along the troughs are smaller. Looking at their time dependence one can see that, in either case, $\tilde{\rho}$ is not periodic in time. This is a distinctive difference between our solutions and those of Alber's equation.

Cases c and d, whose spectral evolution turned out to be milder than cases a and b now exhibit a different behavior of their corresponding variances $\tilde{\rho}$. As seen from Fig. 7a the evolution of case c is similar to that of the previous cases although with smaller values; the crest of $\tilde{\rho}$ is about twice its initial value and, for a fixed $\tilde{x}$, the time evolution is qualitatively periodic comparable with solutions of Alber's equation.

In case d, the one outside the instability boundaries, changes in $\tilde{\rho}$ are much smaller. A snapshot of the variance, although not exactly a sinusoidal, does not seem to deviate far from it and its time dependency seems periodic in this case, see Fig. 7b.

Before closing this section, we look at the variance ρ/ρ_h where ρ_h is the variance of a homogeneous sea state. This function ρ/ρ_h is the key ingredient that will allow us to compute the probabilities of freak waves in the following section.

The homogeneous variance is given by

$$\rho_h = \langle \eta^2 \rangle = \frac{1}{4g\pi^2} \sum_{j=1}^{N} \omega_j C_j = \frac{1}{4g\pi^2} \tilde{H} = \sum_{j=1}^{N} S(k_j)\, dk, \tag{59}$$

where $\tilde{H}$ is the third invariant.

In order to get a clear picture of the time evolution of ρ/ρ_h in the full space–time domain, and owing to the spacial periodicity of the ρ, we shift our results periodically in $\tilde{x}$ in such a way that the maximum always appears along $\tilde{\xi} = 0$. Physical speaking, we are just putting ourselves on a moving reference frame $\tilde{\xi}$, that moves with the speed of the variance letting its maximum remain always on the same position.

In Figs. 8a, 8b, 9a and 9b we plot the level lines of ρ/ρ_h as a function of $\tilde{\xi}$ and $\tilde{t}$ for cases a, b, c and d respectively. In all four cases we show the level lines on the whole domain, the lower left panel shows the initial stages of the evolution and the lower right panel shows the evolution at a later stage. All the contours were slightly smoothed.

In cases a and b we are able to distinguish between two different behaviors happening at different stages of the evolution. At an early stage the level lines of ρ/ρ_h form close loops centered, at times $\tilde{t} \approx 8$ in case a and $\tilde{t} \approx 7$ in case b. We call such loops cycles. During this early stage the evolution is a sequence of consecutive cycles. Such cycles closely resembles the solutions of Alber's equation; they are one recurrent cycle in that case. See Figs. 5 and 7 of Ribal et al. [4].

The second type of behavior, observed in the evolution at a later stage, is not organized by cycles but its distinctive feature is that it maintains larger values for all time. The variance does not return to a state of "rest" as it happens during

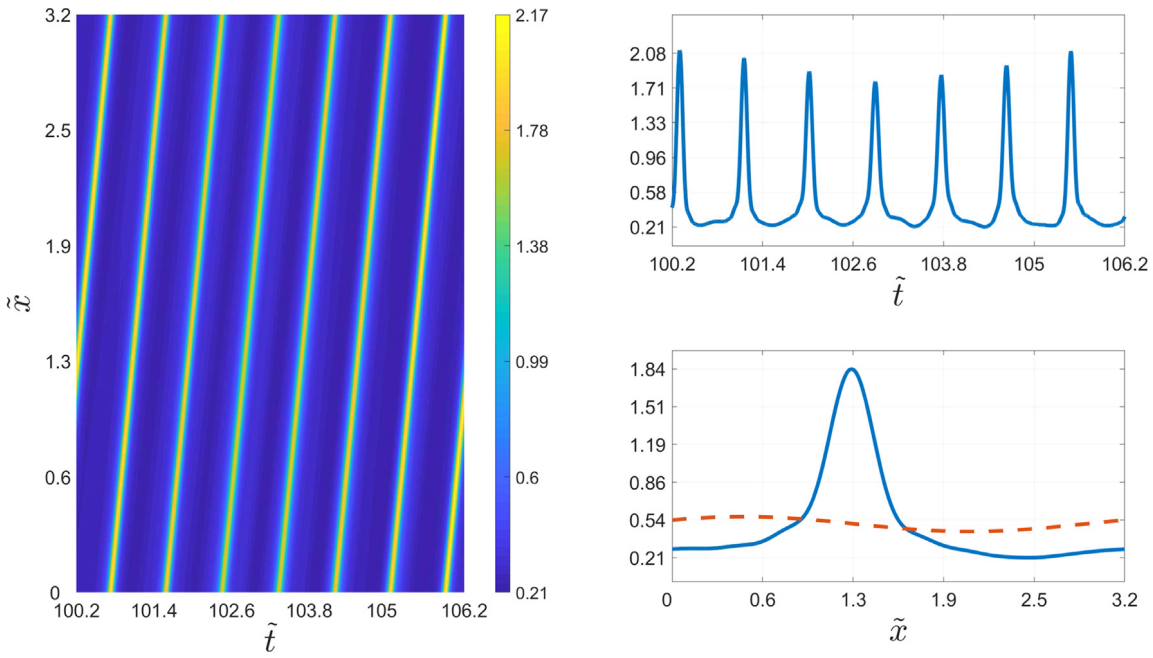

(a) Case a: Evolution of the variance of the free surface.

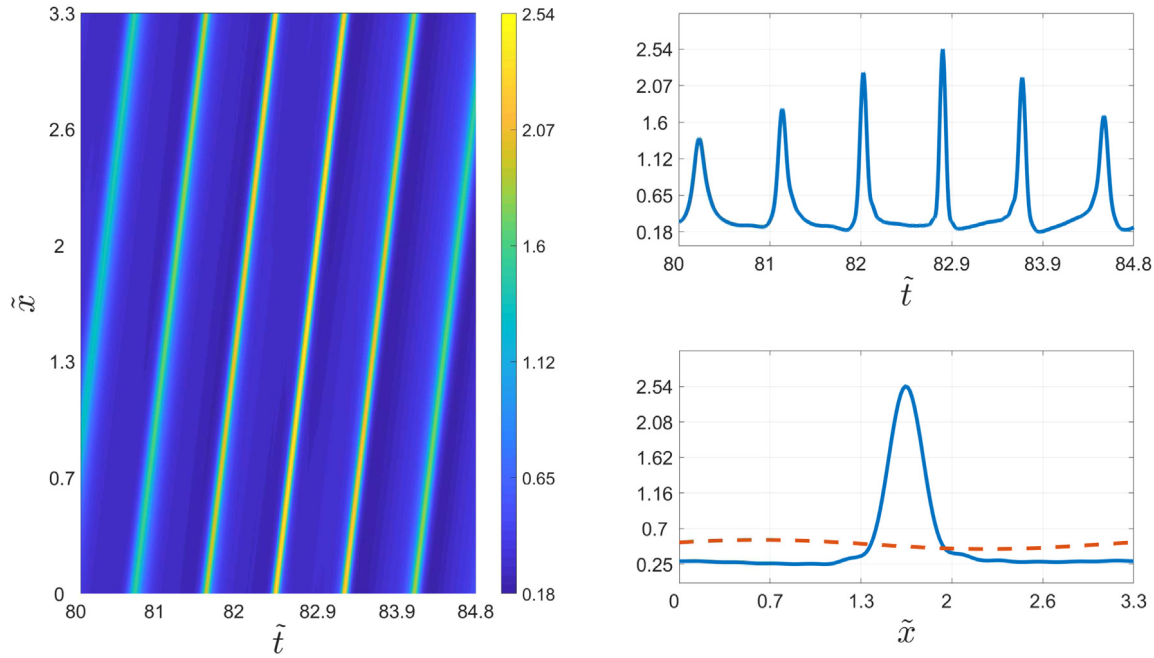

(b) Case b: Evolution of the variance of the free surface.

Fig. 6. Detail of Time evolution of the variance of the free surface elevation along the interval $t = 1000$ s to $t = 1060$ s. The left panel shows the variance of the free surface elevation. On the right panel we plot a horizontal and a vertical section of the variance. The red dashed line on the bottom right is the initial inhomogeneous variance.

the cycles. This can be seen on the lower right panel of Figs. 8a and 8b for cases a and b, respectively. This behavior is as if consecutive cycles were getting closer together and, by means of some "constructive interaction" between them, the

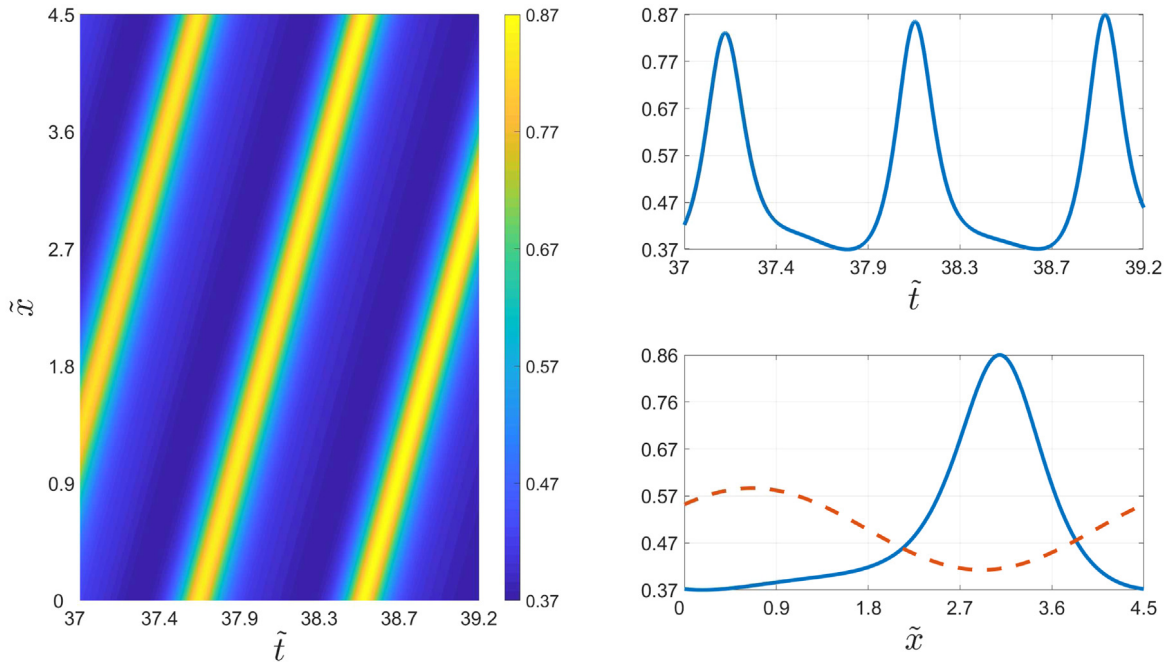

(a) Case c: Evolution of the variance of the free surface.

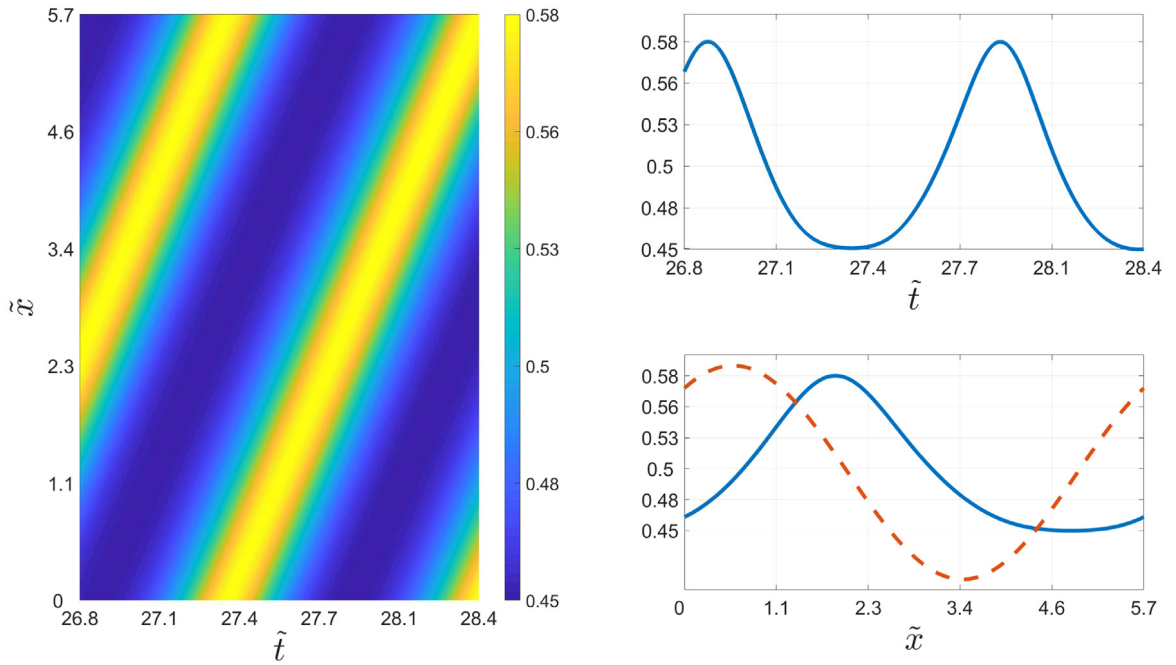

(b) Case d: Evolution of the variance of the free surface.

Fig. 7. Detail of Time evolution of the variance of the free surface elevation along the interval $t = 1000$ s to $t = 1060$ s. The left panel shows the variance of the free surface elevation. On the right panel we plot a horizontal and a vertical section of it. The red dashed line on the bottom right is the initial inhomogeneous variance.

wave field remains "excited". It is during this second stage of the evolution that the variance reaches its largest values of up to 4 times the homogeneous variance in case a, and even 5 times the homogeneous variance in case b.

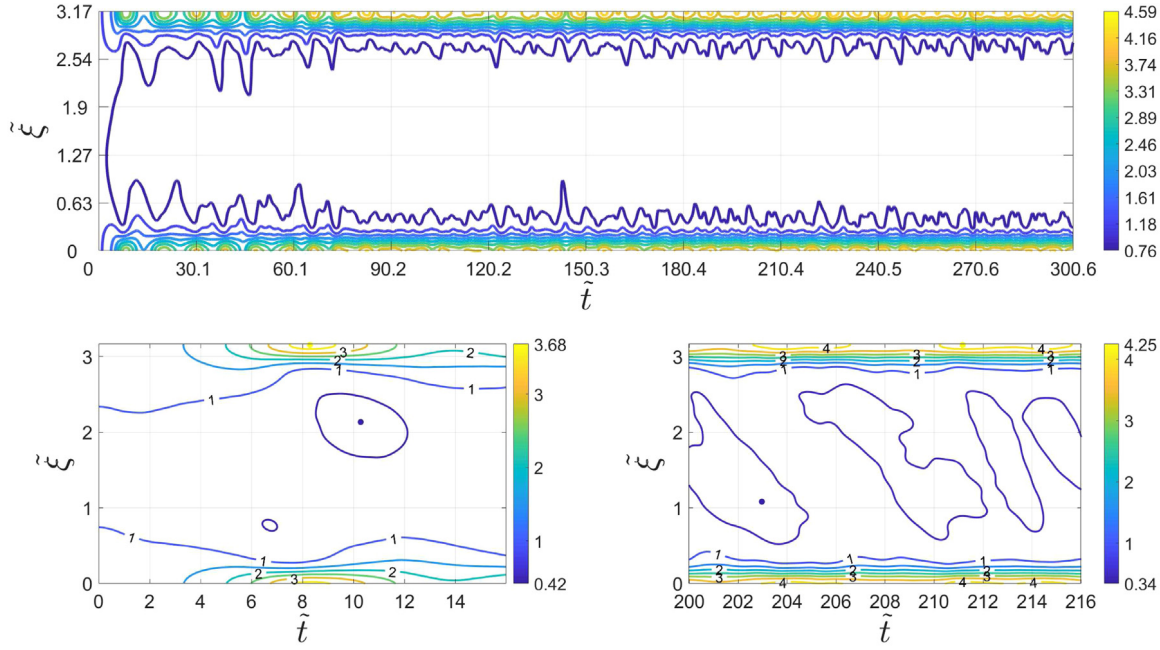

(a) Case a: Time evolution of the variance of the free surface elevation ρ/ρ_h.

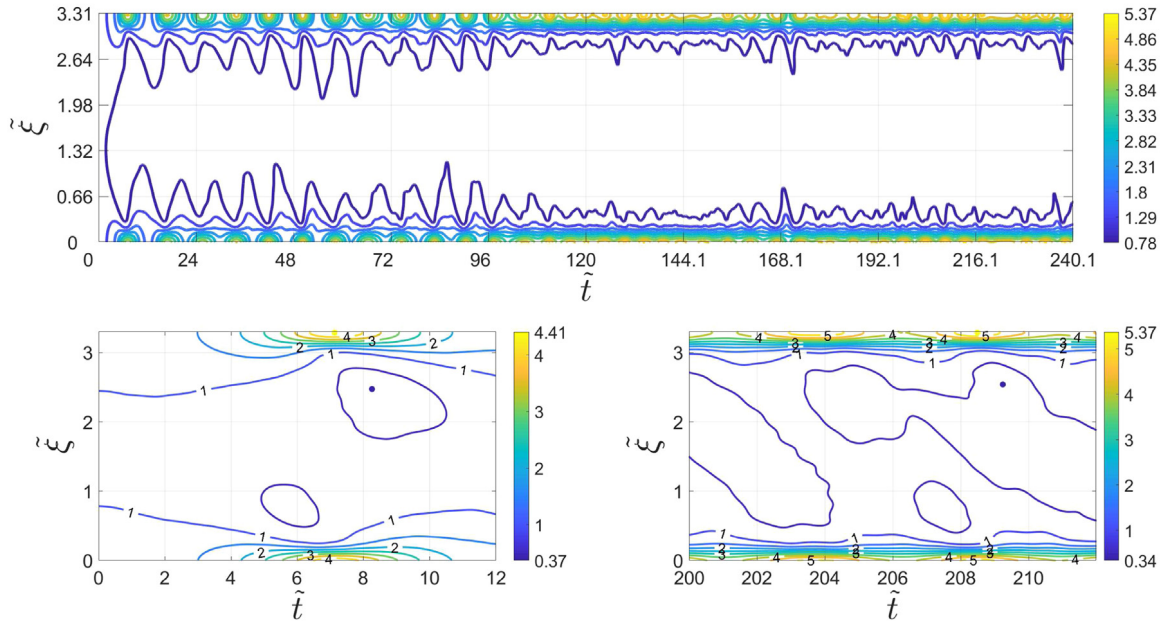

(b) Case b: Time evolution of the variance of the free surface elevation ρ/ρ_h.

Fig. 8. Upper panel: Level lines of the time evolution of the variance of the free surface. Bottom left panel: Details of the first energy exchange cycle. Bottom right panel: Detail of the long time evolution of the variance.

Note that in cases a and b there is a transition period between the two types of behaviors exhibited by the variance of the free surface. For case a the change happens gradually on the time interval $\tilde{t} \approx 45$ up to $\tilde{t} \approx 75$. For case b the transition period goes from $\tilde{t} \approx 90$ to $\tilde{t} \approx 112$. In both cases before the transition period the level lines form well separated loops and after the transition they tend to be more straight.

The evolution of cases c and d is completely described as a sequence of cycles, see Figs. 9a and 9b respectively. Case c resembles the examples treated by Ribal et al. in [4] and case d shows a slower sequence of cycles. The recurrent period

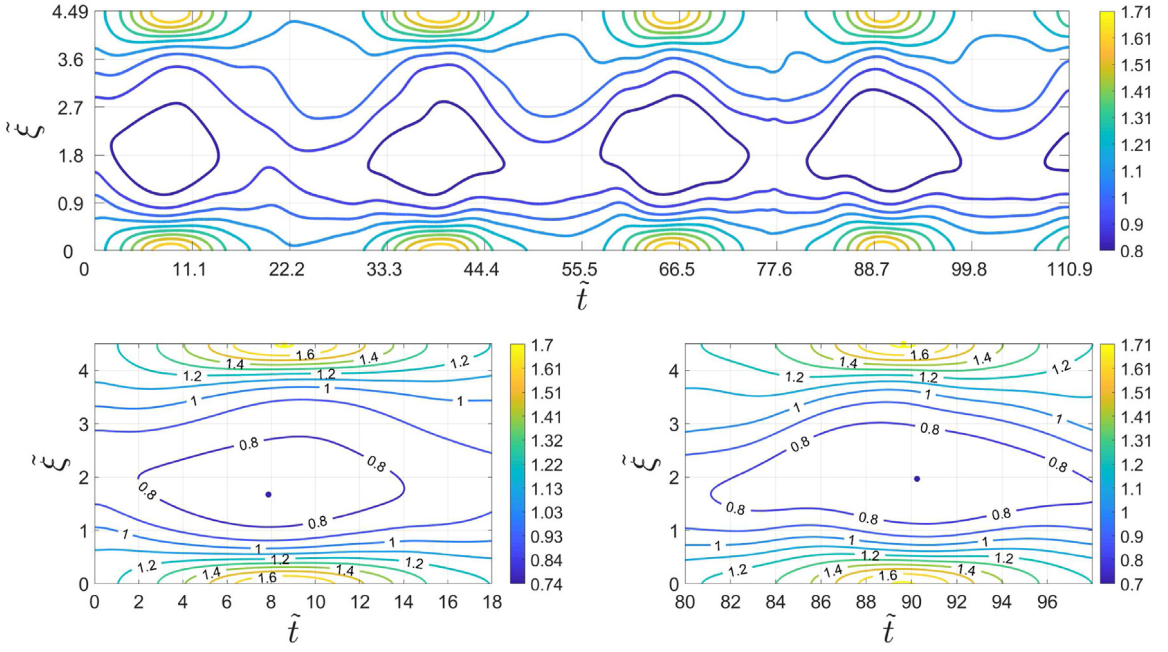

(a) Case c: Time evolution of the variance of the free surface elevation ρ/ρ_h.

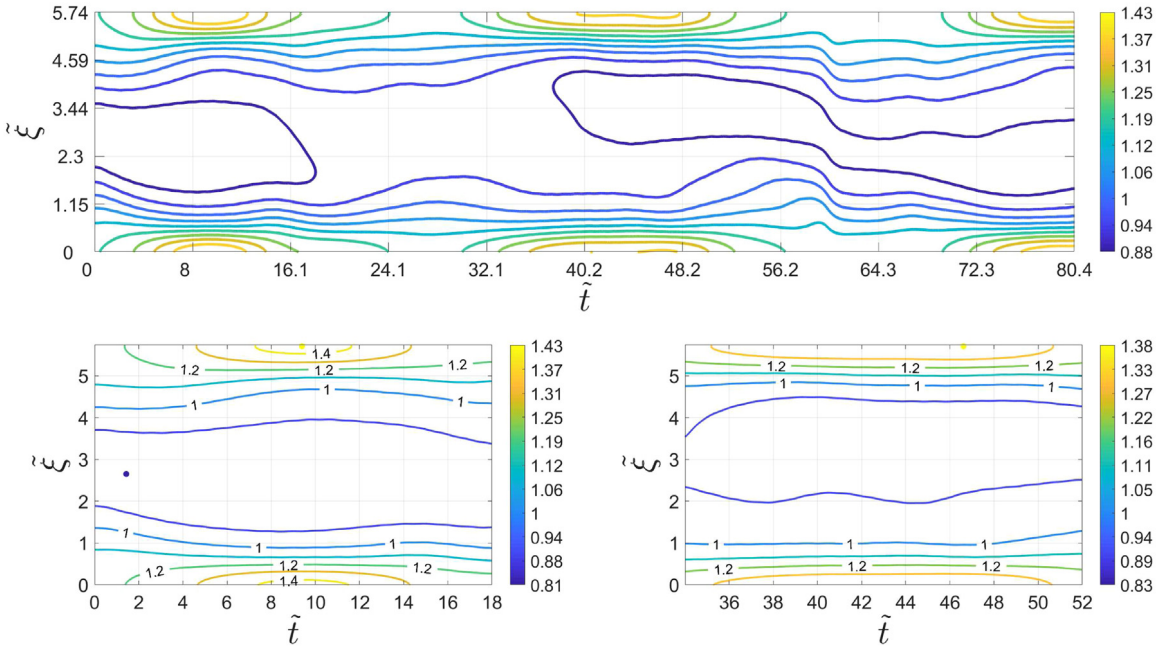

(b) Case d: Time evolution of the variance of the free surface elevation ρ/ρ_h.

Fig. 9. Upper panel: Level lines of the time evolution of the variance of the free surface. Bottom left panel: Details of the first energy exchange cycle. In these cases the variance has a recurrent behavior. Bottom right panel: Detail of a second cycle of the interaction.

of the cycles, in both cases, is roughly $\tilde{t} \approx 18$. It is uncertain at the moment whether the behavior of cases c and d will remain as seen, or it will eventually exhibit a long time evolution akin to that of cases a and b.

Finally we tested the effect of the parameter μ, namely the strength of the initial inhomogeneity. To this end we considered case b with a smaller value of μ. The result is seen in Fig. 10 where we plot the evolution of both variances. The upper panel is the same as in Fig. 8b where $\mu = 0.1$ and the lower panel corresponds to $\mu = 0.01$. As seen from the figure, smaller values of μ lead to an initial "warm up" time similar to the one discovered by Stuhlmeier and Stiassnie

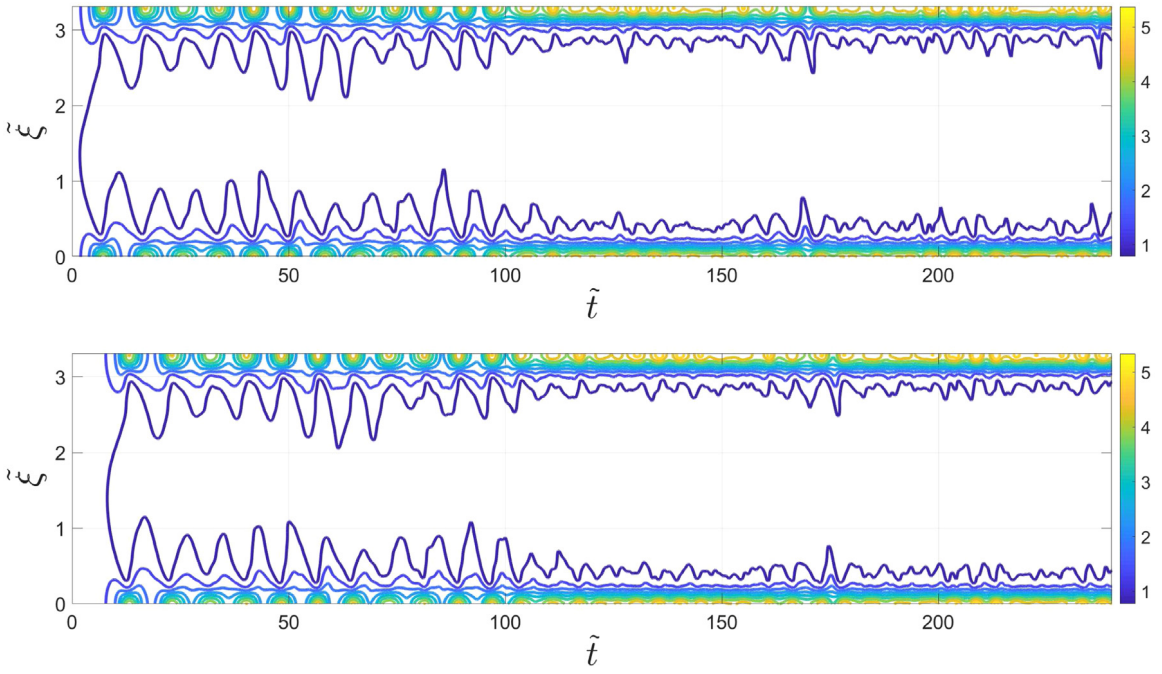

Fig. 10. Time evolution of the variance of the free surface elevation ρ/ρ_h. The upper panel shows case b with $\mu = 0.1$. The lower panel is case b but this time we used $\mu = 0.01$.

in [10]. After the initial delay both solutions are practically indistinguishable from each other, both exhibiting the same qualitative behavior described above.

6. Freak waves' statistics

In this section we study the statistics of an inhomogeneous random sea state. Our goal is to show that the probability of encountering freak waves increases significantly when compared to that of a homogeneous wave field. The formula that will allows us to do so, was derived by Regev et al. see formula 9 in [3]. It has been extensively used to establish statistical properties of inhomogeneous wave fields. Here, for clarity sake, we derive their formula.

Our starting point is that the probability density function of the wave height H, of a narrow banded, homogeneous wave field, is Rayleigh distributed. We refer to Holthuijsen [12] and references therein, for a complete treatment of this subject and the derivation of this result. So,

$$P(H \leq \hat{H}) = 1 - \exp\left(-\frac{\hat{H}^2}{8\rho_h}\right). \tag{60}$$

Here ρ_h is the variance of the (homogeneous) free surface elevation, see formula (59). Note that this formula holds true for every point (x, t), as the variance is constant and stationary for a homogeneous sea state. The probability (60) depends on the root mean square of the wave height, through

$$H_{rms0} = \sqrt{8\rho_h}. \tag{61}$$

Formulas (60) and (61) are extrapolated to the inhomogeneous case, where Regev et al. [3], took the root mean square to be

$$H_{rms}(x, t) = \sqrt{8\rho(x, t)}. \tag{62}$$

Note that it depends on position and time unlike H_{rms0}. Then, the probability that the wave height exceeds a certain value, at a given point (x, t) is given by

$$P(H > \hat{H}) = \exp\left(-\left(\frac{\hat{H}}{H_{rms}}\right)^2\right) = \exp\left(-\left(\frac{\hat{H}}{H_{rms0}}\right)^2 \frac{\rho_h}{\rho}\right). \tag{63}$$

In order to compute such probability, for a region of space and time, one simply averages formula (63) over it. In case of an interval of length L and a time window of duration T, the probability that the wave height H exceeds a given value $\hat{H}$ on that interval during that time is

$$P(H > \hat{H}) = \frac{1}{LT}\int_{x_0}^{x_0+L}\int_{t_0}^{t_0+T} \exp\left(-\left(\frac{\hat{H}}{H_{rms0}}\right)^2 \frac{\rho_h}{\rho(x,t)}\right) dxdt. \tag{64}$$

Here x_0, t_0, L and T define the intervals of interest.

Owing to the periodicity in x of ρ one usually considers one period of the solution, so $x_0 = 0$ and $L = 2\pi/K^{(max)}$. As our solution is not periodic in time, we used different time windows to establish the probabilities of the freaks waves in cases a, b, c, and d.

Recalling that a freak wave is a wave whose wave height is larger than twice the significant wave height H_s, which can be estimated as

$$H_s \approx \sqrt{2}H_{rms0}. \tag{65}$$

In Fig. 11 we plot the probabilities obtained, for cases a, b, c and d, using different time windows. In this figure the blue solid line corresponds to case a, the yellow line with dots to case b, the red dashed line to case c, and the purple broken line with dots to case d. The black line with triangles shows the values of the Rayleigh distribution. The values on the x-axis range from $2.85H_{rms0} \approx 2H_s$ to $4.56H_{rms0}$, so all the values correspond to freak waves. The blue stars correspond to the probabilities for case a, obtained by Ribal et al. see example B_4 in [4]. Note that in all cases the C.S.Y. equation predicts higher probabilities of encountering freak waves than those predicted by the Rayleigh distribution, and even those obtain from Alber's equation.

The first time window that we used, is the duration of the first cycle of ρ/ρ_h, exactly as plotted on the bottom left panel of Figs. 8a–9b. The corresponding probabilities are plotted on the first panel of Fig. 11. The second time window was at a later stage in the evolution. Exactly the one plotted in the bottom right panel of Figs. 8a–9b. The probabilities in this case are plotted in the middle panel of Fig. 11. The probabilities on the third panel were computed using the whole simulated domain.

The probabilities of encountering waves higher than twice and thrice the significant wave height are given in Table 3.

Looking at cases a and b, the cases where the instability is stronger, there is a general increase in the probability of the freak waves, see Fig. 11. Such probabilities depend on the type of behavior of the evolution taken into consideration. Indeed Table 3 shows a significant increase of the probabilities when one considers the second type of behavior, which happens at later stage, than that of the recurrent type of behavior, which happens at an early stage of the evolution.

Note that for cases c and d there is no significant change in the probabilities, as seen in Fig. 11. This is a consequence of the recurrent behavior of the evolution which remained during the whole time of the simulation.

The results obtain for case a are slightly larger than those of case B_4 obtained by Ribal et al. [4]. Their results are plotted with blue stars in Fig. 11. The prediction based on Alber's equation is that 205 out of 10^5 waves have a significant wave height larger than twice H_s. On the other hand during the first cycle of case a the C.S.Y. equation predicts about a 50% increase with 390 waves out of 10^5. The increase is more pronounced if one considers the later stages of the evolution, with 114 out of 10^4, about five times larger than that from Alber's equation. For waves higher than thrice the significant wave height we obtained 109 out of a million waves, during the first cycle, and a seven times increase later on. For this case Alber's equation predicted only 21 out of a million.

We close this section by noting that formula (64) looks different to formula 9 of Regev et al. [3]. Nevertheless both formulas define the same probability for the wave height over a region of space and time and can be shown to be identical.

7. Discussion and conclusions

One of the questions that motivated this article was, the claim that any spectra stabilizes as it broadens. Here we found that indeed a JONSWAP spectrum is unstable when it is narrow (large values of γ) and it stabilizes as it broadens $\gamma \to 1$, as predicted from Alber's equation. Nevertheless, this conclusion now comes from a broad band model, thus establishing its validity in a more general and realistic framework. Moreover, our results show that Alber's equation captures accurately the instability region, in particular if one uses Gramstad's fit [5].

We have tried one example (not presented) inside the stability region, e.g. $\gamma = 2$, $\alpha = 0.012$, and the resulting simulation turned out to be constant in time. We did not observe any decay in the inhomogeneous perturbation during this case.

The major difference between our results and those of Ribal et al. and Stiassnie et al. [2,4] appears in the time evolution of the variance of the free surface. Initially, after a warm up time (which is connected to the intensity of the initial disturbance), the evolution can be described as a sequence of cycles, analog to the behavior of the solutions of Alber's equation. Each cycle starts with a slowly varying variance indicating that wave field is in a relaxed state. Then it localizes, its crest gets taller and larger whereas its trough gets smaller and flatter, before going back to a "relaxed" state. This recurrent type of behavior happens during the early stages of the evolution for cases a and b, but remained for cases c and d throughout the evolution.

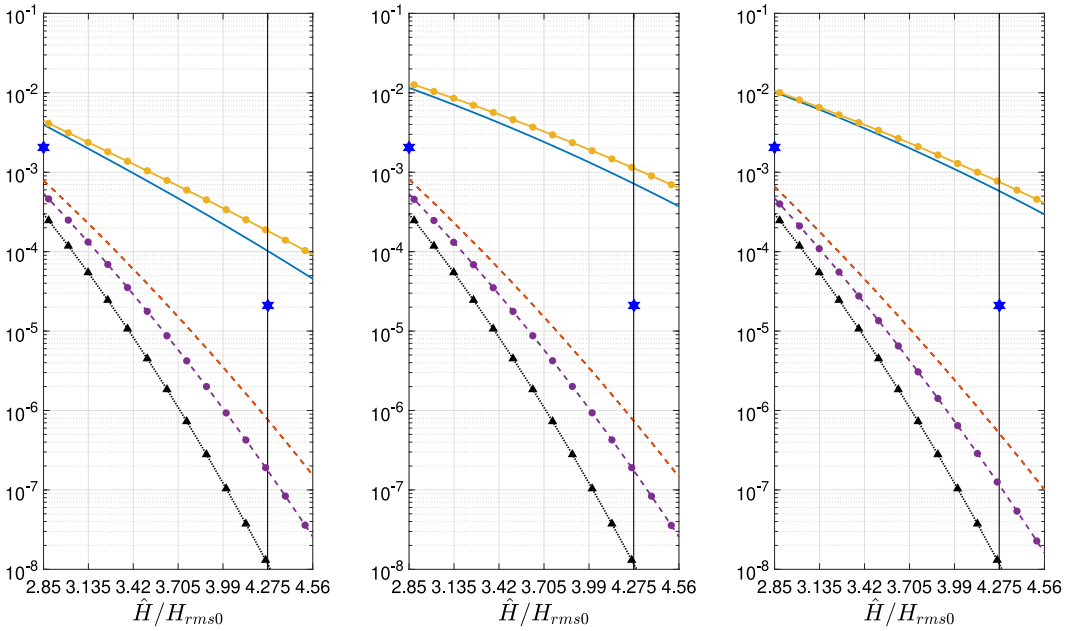

Fig. 11. $P\left(H/H_{rms0} > \hat{H}/H_{rms0}\right)$. The black line with triangles corresponds to the Rayleigh distribution for purely homogeneous sea states. The blue solid line corresponds to case a, the yellow line with dots to case b, the red broken line to case c and the purple broken line with dots to case d. Left panel: probabilities obtained during the first cycle of the evolution. Middle panel: probabilities obtained during a later stage. Right panel: probabilities obtained using the whole simulated domain, 3000 s of the evolution. The blue stars are the results predicted by Alber's equation for case a. The vertical line is $H_{rms0} = 3H_s$.

Table 3
Probabilities of encountering freak waves in cases a, b,c and d. In each case, the early and late stages refer to the time intervals in Figs. 8(a)–9(b), respectively. "Whole" means that we used the entire computed domain to calculate the probabilities.

Cases	$P(H > 2H_s)$		
	Early stage	Late stage	Whole
Case a	0.0039	0.0114	0.0101
Case b	0.0044	0.0131	0.0105
Case c	7.6086×10^{-4}	7.8717×10^{-4}	6.3854×10^{-4}
Case d	5.20157×10^{-4}	5.1415×10^{-4}	4.5188×10^{-4}
Rayleigh		2.8493×10^{-4}	
Cases	$P(H > 3H_s)$		
	Early stage	Late stage	Whole
case a	1.0964×10^{-4}	7.6016×10^{-4}	6.1436×10^{-4}
case b	1.9381×10^{-4}	0.0012	7.9539×10^{-4}
case c	8.8408×10^{-4}	9.54017×10^{-7}	5.94267×10^{-7}
case d	2.0648×10^{-7}	2.0668×10^{-7}	1.3675×10^{-7}
Rayleigh		1.1742×10^{-8}	

In the most unstable cases such cycles get closer together resulting in a sea state that is continuously "excited" and does not seem to go back to a "relaxed" state. This second type of behavior is the main feature observed in the long time evolution of the most unstable cases.

Interestingly, this was observed in the narrower cases (a and b); whereas for the broader examples (cases c and d) the recurrent behavior was dominant.

The evolution of the variance clearly impacts the statistics of the underlying wave field. During the early cycles the probabilities of encountering freak waves are in general agreement with predictions made with Alber's equation. However they get significantly larger when the variance enters into the "excited" state. This behavior was observed only for cases a and b at larger times of their evolution.

There is still a major problem which demands further research. All predictions made by the inhomogeneous models require that, at some point, an external inhomogeneous disturbance enters the system. The challenge here is to find a physical mechanism capable of correlating the wave components in the ocean. It is our current belief that further research

into this topic may render inhomogeneous models a suitable "companion" of the kinetic equation, currently used in wave forecasting models.

CRediT authorship contribution statement

David Andrade: Methodology, Software, Investigation, Writing - original draft, Writing - review & editing. **Michael Stiassnie:** Conceptualization, Investigation, Resources, Writing - review & editing, Project administration, Funding acquisition.

Declaration of competing interest

The authors declare that they have no known competing financial interests or personal relationships that could have appeared to influence the work reported in this paper.

Acknowledgment

The authors are grateful to Dr. R. Stuhlmeier from the University of Plymouth for fruitful discussions related to this work.

This research was supported by the Israel Science Foundation (**Grant 261/17**).

References

[1] I.E. Alber, The effects of randomness on the stability of two-dimensional surface wavetrains, Proc. R. Soc. A: Math. Phys. Eng. Sci. 363 (1715) (1978) 525–546, http://dx.doi.org/10.1098/rspa.1978.0181.
[2] M. Stiassnie, A. Regev, Y. Agnon, Recurrent solutions of Alber's equation for random water-wave fields, J. Fluid Mech. 598 (2008) http://dx.doi.org/10.1017/s0022112007009998.
[3] A. Regev, Y. Agnon, M. Stiassnie, O. Gramstad, Sea swell interaction as a mechanism for the generation of freak waves, Phys. Fluids 20 (11) (2008) 112102, http://dx.doi.org/10.1063/1.3012542.
[4] A. Ribal, A.V. Babanin, I. Young, A. Toffoli, M. Stiassnie, Recurrent solutions of the Alber equation initialized by joint north sea wave project spectra, J. Fluid Mech. 719 (2013) 314–344, http://dx.doi.org/10.1017/jfm.2013.7.
[5] O. Gramstad, Modulational instability in jonswap sea states using the alber equation, in: ASME 2017 36th International Conference on Ocean, Offshore and Arctic Engineering, American Society of Mechanical Engineers Digital Collection, 2017.
[6] A.G. Athanassoulis, G.A. Athanassoulis, M. Ptashnyk, T.P. Sapsis, Strong solutions for the Alber equation and stability of unidirectional wave spectra, Kinetic & Related Models 13 (2020) 703–737, http://dx.doi.org/10.3934/krm.2020024.
[7] D.R. Crawford, P.G. Saffman, H.C. Yuen, Evolution of a random inhomogeneous field of nonlinear deep-water gravity waves, Wave Motion 2 (1) (1980) 1–16, http://dx.doi.org/10.1016/0165-2125(80)90029-3.
[8] C.C. Mei, M.A. Stiassnie, D.K.-P. Yue, Theory and Applications of Ocean Surface Waves: Part 2: Nonlinear Aspects, third ed., World Scientific, 2018.
[9] R. Stuhlmeier, T. Vrecica, Y. Toledo, Nonlinear wave interaction in coastal and open seas: Deterministic and stochastic theory, in: D. Henry, K. Kalimeris, E.I. Părău, J.-M. Vanden-Broeck, E. Wahlén (Eds.), Nonlinear Water Waves, Birkhäuser Basel, 2019.
[10] R. Stuhlmeier, M. Stiassnie, Evolution of statistically inhomogeneous degenerate water wave quartets, Phil. Trans. R. Soc. A 376 (2111) (2019) 20170101, http://dx.doi.org/10.1098/rsta.2017.0101.
[11] V.P. Krasitskii, On reduced equations in the hamiltonian theory of weakly nonlinear surface waves, J. Fluid Mech. 272 (1994) 1–20.
[12] L.H. Holthuijsen, Waves in Oceanic and Coastal Water, Cambridge university press, 2010.